Target detection within sea clutter: a comparative study by fractal scaling analyses

Jing Hu[1], Jianbo Gao[1], Fred L. Posner[2], Yi Zheng[1], and Wen-wen Tung[3]
[1]Department of Electrical and Computer Engineering,
University of Florida, Gainesville, FL 32611
[2]Naval Research Laboratory, Radar Division, Code 5313,
4555 Overlook Avenue SW, Washington, DC 20375
[3]Department of Earth & Atmospheric Sciences,
Purdue University, West Lafayette, IN 47907
Email: jhu@ecel.ufl.edu, gao@ece.ufl.edu

Abstract

Sea clutter refers to the radar returns from a patch of ocean surface. Accurate modelling of sea clutter and robust detection of low observable targets within sea clutter are important problems in remote sensing and radar signal processing applications. Due to lack of fundamental understanding of the nature of sea clutter, however, no simple and effective methods for detecting targets within sea clutter have been proposed. To help solve this important problem, we apply three types of fractal scaling analyses, fluctuation analysis (FA), detrended fluctuation analysis (DFA), and the wavelet-based fractal scaling analysis to study sea clutter. Our analyses show that sea clutter data exhibit fractal behaviors in the time scale range of about 0.01 sec to a few seconds. The physical significance of these time scales is discussed. We emphasize that time scales characterizing fractal scaling break are among the most important features for detecting patterns using fractal theory. By systematically studying 392 sea clutter time series measured under various sea and weather conditions, we find very effective methods for detecting targets within sea clutter. Based on the data available to us, the accuracy of these methods is close to 100%.

Keywords: Fractal, Pattern Recognition, Sea Clutter, Target Detection

1 Introduction

Sea clutter is the backscattered returns from a patch of the sea surface illuminated by a radar pulse. Accurate modelling of sea clutter and robust detection of low observable targets within sea clutter are important problems in remote sensing and radar signal processing applications, for a number of reasons: (i) identifying objects within sea clutter such as submarine periscopes, low-flying aircrafts, and missiles can greatly improve coastal and national security; (ii) identifying small marine vessels, navigation buoys, small pieces of ice, patches of spilled oil, etc. can significantly reduce the threat to the safety of ship navigation; (iii) monitoring and policing of illegal fishing is an important activity in environmental monitoring. Since sea clutter is a type of electromagnetic wave, sea clutter study may also help understand fading and non-Gaussian noise in wireless communications, so that wireless communication channel characterization and signal detection can be greatly improved.

Due to massive reflection of radar pulses from wavy or even turbulent ocean surfaces, sea clutter is often highly non-Gaussian [1–8], even spiky [9], especially in heavy sea conditions. Hence, sea clutter modelling is a very difficult problem, and a lot of effort has been made to study sea clutter. Traditionally, sea clutter is often studied in terms of certain simple statistical features, such as the marginal probability density function (pdf). The non-Gaussian feature of sea clutter has motivated researchers to employ Weibull [1], log-normal [2–4], K [5–7, 10], and compound-Gaussian [8] distributions to model sea clutter. However, such simple phenomenological modelling of sea clutter only offers limited analytical or physical understanding.

To gain deeper understanding of the nature of sea clutter, the concept of fractal has been employed for the modelling of the roughness of sea surface and investigation of scattering from rough surface [11–13]. Possible chaotic behavior of sea clutter has also been studied [14–21].

Since the ultimate goal of sea clutter study is to improve detection of targets embedded within clutters, a lot of effort has been made to design innovative methods for target detection within sea clutter. Notable methods include time-frequency analysis techniques [22], wavelet based approaches [23], neural network based approaches [24–26], and wavelet-neural net combined ap-

proaches [27], as well as utilizing the concept of fractal dimension [28] and fractal error [29, 30], and multifractal analysis [31, 32]. Note that most of the above works were based on the analysis of radar images. To improve detection accuracy, some researchers resort to higher resolution more powerful millimeter wave radars [33]. The status of the field clearly indicates that one needs to adopt a systematic approach, work on a large number of datasets measured under various sea and weather conditions, and design a few readily computable parameters that can accurately and easily detect targets within sea clutter.

In this paper, we employ methods from random fractal theory to study sea clutter. Specifically, we apply three types of fractal scaling analyses, fluctuation analysis (FA), detrended fluctuation analysis (DFA), and the wavelet-based fractal scaling analysis to analyze three types of data, the measured sea clutter amplitude data $u(n)$, the data $v(n)$ obtained by integrating $u(n)$, and the data $w(n)$ obtained by differencing $u(n)$. These analyses show that sea clutter data exhibit fractal behaviors in the time scale range of about 0.01 sec to a few seconds. By systematically studying 392 sea clutter time series measured under various sea and weather conditions, we find very effective methods for detecting targets within sea clutter by applying FA to $u(n)$, DFA to both $u(n)$ and $v(n)$, and the wavelet-based approach to all three types of data. Based on the available data, the accuracy of these detectors is found to be close to 100%.

The remainder of the paper is organized as follows. In Sec. 2, we briefly describe the sea clutter data. In Sec. 3, we introduce the three types of fractal scaling analyses, FA, DFA and the wavelet-based fractal scaling analysis. In Sec. 4, we apply the three types of fractal scaling analyses to analyze the three types of data mentioned above, and make careful comparisons among the three types of analyses. Finally, some concluding remarks are made in Sec. 5.

2 Sea clutter data

14 sea clutter datasets were obtained from a website maintained by Professor Simon Haykin: http://soma.ece.mcmaster.ca/ipix/dartmouth/datasets.html. The measurement was made using the McMaster IPIX radar at the east coast of Canada, from a clifftop near Dartmouth, Nova Scotia. The operating (or carrier) frequency of the radar was 9.39 GHz (and hence a wavelength of about

3 cm). The grazing angle varied from less than 1^0 to a few degrees. The wave height in the ocean varied from 0.8 m to 3.8 m (with peak height up to 5.5 m). The wind conditions varied from still to 60 km/hr (with gusts up to 90 km/hr). Data of two polarizations, HH (horizontal transmission, horizontal reception) and VV (vertical transmission, vertical reception), were analyzed here. Each dataset contains 14 spatial range bins of HH as well as 14 range bins of VV datasets. Therefore, there are a total of 392 sea clutter time series. A few of the range bins hit a target, which was made of a spherical block of styrofoam of diameter 1 m, wrapped with wire mesh. This is a very small target, more difficult to detect than, say, a ship. Usually, the range bin where the target is strongest is labeled as primary target bin, and the neighboring range bins where the target may also be visible labeled as secondary target bins. However, due to the drift of the target, it is possible that the target in a primary range bin may not be the strongest and some secondary target bins may not hit the target at all. Each range bin data contains 2^{17} complex numbers, with a sampling frequency of 1000 Hz. We analyze the amplitude data. Fig. 1 shows two examples of the sea clutter amplitude data without and with target. Note that similar signals have been observed in many different fields. Therefore, the analysis used in this paper may also be applicable to those fields.

3 Fractal scaling analysis

In this section, we describe one of the prototypical models for random fractals — the fractional Brownian motion (fBm) model, then present the three types of fractal scaling analyses.

3.1 Fractional Brownian motion (fBm)

FBm $B_H(t)$ is a Gaussian process with mean 0, stationary increments, variance

$$E[(B_H(t))^2] = t^{2H} \tag{1}$$

and covariance:

$$E[B_H(s)B_H(t)] = \frac{1}{2}\{s^{2H} + t^{2H} - |s-t|^{2H}\} \tag{2}$$

where H is the Hurst parameter. The increment process of fBm, $X_i = B_H(i+1) - B_H(i),\ i \geq 1$, is called fractional Gaussian noise (fGn) process. It is a zero mean, stationary Gaussian time series.

Noting that

$$E(X_iX_{i+k}) = E\{[B_H(i+1) - B_H(i)][B_H(i+1+k) - B_H(i+k)]\},$$

by Eq. (2), one can easily obtain the autocovariance function $\gamma(k)$ for the fGn process:

$$\gamma(k) = \frac{1}{2}\{(k+1)^{2H} - 2k^{2H} + |k-1|^{2H}\},\ k \geq 0 \tag{3}$$

hence,

$$\gamma(k) \sim k^{2H-2} \quad \text{as} \quad k \to \infty, \tag{4}$$

When $H = 1/2$, the process is called memoryless or short range dependent, the most well-known example being white Gaussian noise and its integration being the standard Brownian motion process. When $0 < H < 1/2$, we have negatively correlated increments; a jump up is more likely followed by a jump down and vice-versa. When referring to fBm, this is called "anti-persistence" by Mandelbrot [34]. For $1/2 < H < 1$, we have positively correlated increments. This means that a jump tends to be followed by another jump in the same direction. In fBm, this is called "persistence" [34]. Such processes have long memory properties.

By the Wiener-Khinchin theorem, one finds that the power spectral density (PSD) for the fGn process follows a power-law,

$$E_X(f) \sim 1/f^{2H-1}. \tag{5}$$

Furthermore, the PSD for the fBm $B_H(t)$ time series is of the form

$$E_{B_H(t)}(f) \sim 1/f^{2H+1}. \tag{6}$$

The processes under study are thus often called $1/f^{\alpha}$ noise. Such type of noise is very ubiquitous. For classic examples, we refer to [35–37]. More recently, it has been found that network traffic [38–40], DNA sequence [41–43], human cognition [44], ambiguous visual perception [45], coordination [46], posture [47], dynamic images [48, 49], the distribution of prime numbers [50], etc., all belong to such type of stochastic processes. It is further observed that principle component analysis of such processes leads to power-law decaying eigen-value spectrum [51].

For a general random-walk-type $1/f^{\alpha}$ process (i.e., not necessarily Gaussian process) with $1 < \alpha < 3$, it can be proven that [52, 53]

$$\alpha = 2H + 1 \tag{7}$$

We shall see later that Eq. (7) may hold for a wider range of α or H, depending on which method is employed to analyze a dataset. However, when H does not belong to the unit interval, then one cannot say the process to have persistent or anti-persistent correlations.

Note that while in principle Eq. (5) or (6) may be used to estimate the Hurst parameter, when the power-law-like PSD is only valid for a limited frequency range, it may be difficult to determine a suitable region to define the power-law scaling by this approach. This point will be made more concrete later.

3.2 Fluctuation analysis (FA)

FA characterizes the second order statistic—the correlation, in a time series. It works as follows. We consider a covariance stationary stochastic process $X = \{X(i), i = 1, 2, \cdots\}$. A stochastic process is covariance stationary if it has constant mean μ = E$[X(i)]$, finite variance σ^2 = E$[(X(i) - \mu)^2]$, and covariance E$[(X(i) - \mu)(X(i+k) - \mu)]$ that depends only on k. We first subtract the mean μ from the time series. Denote the new time series as $x = \{x(i), i = 1, 2, \cdots\}$, where

$$x(i) = X(i) - \mu.$$

Then we form the partial summation of x to construct a new time series $y = \{y(n), n = 1, 2, \cdots\}$, where

$$y(n) = \sum_{i=1}^{n} x(i). \tag{8}$$

Often, y is called a "random walk" process of x, while x an "increment" process. One then examines whether the following scaling laws hold or not,

$$F(m) = \sqrt{\langle |y(n+m) - y(n)|^2 \rangle} \sim m^H, \tag{9}$$

where the average $< \cdot >$ is taken over all possible pairs of $(y(n+m), y(n))$. The parameter H is called the Hurst parameter. When the scaling law described by Eq. (9) holds, the process under investigation is said to be a fractal process.

3.3 Detrended fluctuation analysis (DFA)

When a measured dataset contains some trends (say, linear), it is advantageous to employ DFA [54, 55] instead of FA. Since a lot of ocean waves of different wavelength contribute to the complexity of sea clutter, it is desirable to examine whether DFA may give additional information on the nature of sea clutter. When applying DFA, one works on a random-walk-type process, as described by Eq. (8). It involves the following steps. First one divides the time series into $\lfloor N/m \rfloor$ non-overlapping segments (where the notation $\lfloor x \rfloor$ denotes the largest integer that is not greater than x), each containing m points; then one calculates the local trend in each segment to be the ordinate of a linear least-squares fit for the random walk in that segment, and computes the "detrended walk", denoted by $y_m(n)$, as the difference between the original walk $y(n)$ and the local trend; finally, one examines if the following scaling behavior (i.e., fractal property) holds or not:

$$F_d(m) = \sqrt{< \sum_{n=1}^{m} |y_m(n)|^2 >} \sim m^H \tag{10}$$

where the angle brackets denote ensemble average of all the segments. For ideal fractal processes, FA and DFA yield equivalent results [52]. In practice, when the data under study contains certain trends or is non-stationary, DFA often works more reliably.

3.4 Wavelet-based fractal scaling analysis

The wavelet-based fractal scaling analysis is based on the coefficients of a discrete wavelet decomposition. It involves a scaling function ϕ_0 and a mother wavelet ψ_0. The scaling function satisfies

$$\int_{-\infty}^{\infty} \phi_0(n) dn = 1.$$

The wavelet ψ_0 must have zero average and decay quickly at both ends [56]. The scaled and shifted versions of ϕ_0 and ψ_0 are given by

$$\phi_{j,k}(n) = 2^{-j/2}\phi_0(2^{-j}n - k), \;\; \psi_{j,k}(n) = 2^{-j/2}\psi_0(2^{-j}n - k), \;\; j,k \in Z,$$

where j and k are the scaling (dilation) and the shifting (translation) index, respectively. Different value of j corresponds to analyzing a different resolution level of the signal. One popular technique

used to perform the discrete wavelet transform (DWT) is the multiresolution analysis (MRA). The procedure of performing MRA is detailed as follows [56]:

(1) At the $j = 1$– th resolution, for each $k = 0, 1, 2, \cdots$, compute the approximation coefficient $a_x(j,k)$ and the detailed coefficient $d_x(j,k)$ according to the following formula:

$$a_x(j,k) = \sum_n x(n)\phi_{j,k}(n) = \sum_n x(n)2^{-j/2}\phi_0(2^{-j}n-k)$$

$$d_x(j,k) = \sum_n x(n)\psi_{j,k}(n) = \sum_n x(n)2^{-j/2}\psi_0(2^{-j}n-k)$$

(2) The signal approximation SA_j and the signal detail SD_j at the j-th resolution level are computed as

$$SA_j = \sum_k a_x(j,k)\phi_{j,k}(n)$$

$$SD_j = \sum_k d_x(j,k)\psi_{j,k}(n)$$

(3) Repeat steps (1) and (2) for the $(j+1)$-th resolution level, using the signal approximation SA_j obtained in step (2) as the input signal.

Let the maximum scale resolution level chosen for analysis be J. The signal can be reconstructed using the following equation [56]:

$$x(n) = SA_J + \sum_{j=1}^{J} SD_j = \sum_k a_x(J,k)\phi_{J,k}(n) + \sum_{j=1}^{J}\sum_k d_x(j,k)\psi_{j,k}(n). \tag{11}$$

The first term represents the approximation at level J, and the second term represents the details at resolution level J and lower. MRA builds a pyramidal structure that requires an iterative application of the scaling and the wavelet functions, respectively. This is schematically shown in Fig. 2.

To make the above procedure more concrete, let us take the Haar wavelet as an example. The scaling function and the mother wavelet of the Haar wavelet are defined as

$$\phi_0(n) = \begin{cases} 1, & 0 \le n < 1, \\ 0, & \text{elsewhere.} \end{cases}$$

$$\psi_0(n) = \begin{cases} 1, & 0 \le n < 1/2, \\ -1, & 1/2 \le n < 1, \\ 0, & \text{elsewhere.} \end{cases}$$

They are shown in Fig. 3. We consider the signal $x(n)$ consisting of noisy blocks, as shown in Fig. 4(a). The signal approximations and details at resolution levels 1 through 3 are shown in Figs. 4(b,d,f) (left column) and Fig. 4(c,e,g) (right column), respectively. We have

$$x(n) = SA_1 + SD_1 = SA_2 + SD_2 + SD_1 = SA_3 + SD_3 + SD_2 + SD_1.$$

Let

$$\Gamma(j) = \frac{1}{n_j} \sum_{k=1}^{n_j} |d_x(j,k)|^2 ,$$

where n_j is the number of coefficients at level j, then the Hurst parameter is given by

$$\log_2 \Gamma(j) = (2H-1)j + c_0, \tag{12}$$

where c_0 is some constant. When $\log_2 \Gamma(j)$ vs. the scale j curve is approximately linear for certain range of j, the process $x(t)$ is said to be fractal, with slope being $2H-1$. In particular, a flat horizontal line corresponds to $H = 1/2$.

Recalling that when applying FA or DFA, one works on a random-walk-type process. When one employs the wavelet-based fractal scaling analysis, one works on the original time series. When this is the case, the Hurst parameters estimated by the three methods would be consistent. However, if one also applies the wavelet-based fractal scaling analysis to the random walk process, then the estimated scaling exponent would be $H+1$, where H is obtained by either FA or DFA (when they are equivalent). This point will be made clearer in Sec. 4.

4 Fractal scaling analyses of sea clutter

Given a measured sea clutter data, one does not know a priori whether the original data should be treated as a random-walk-type process or as an increment process. For this reason, we analyze three types of data, the original data, the integrated data, and the differenced data. Let us denote the original sea clutter amplitude data by $u(n), n = 1, 2, \cdots$. The integrated data $v(n)$ is obtained by first removing the mean value $\bar{u}$ and then forming the partial summation,

$$v(n) = \sum_{i=1}^{n} [u(i) - \bar{u}], \quad n = 1, 2, \cdots. \tag{13}$$

The differenced data $w(n)$ is defined as

$$w(n) = u(n+1) - u(n), \quad n = 1, 2, \cdots. \tag{14}$$

We first discuss FA of these three types of data.

4.1 Fluctuation analysis of sea clutter

For notational clarity, we re-denote $F(m)$ in Eq. (9) by $F_{(u)}(m)$, $F_{(v)}(m)$, or $F_{(w)}(m)$, depending on whether FA is applied to the $u(n)$, $v(n)$, or $w(n)$ time series.

4.1.1 Analysis of original sea clutter data

Let us apply FA to the original sea clutter amplitude data $u(n)$ first. We can directly apply Eq. (9) by replacing $y(n)$ by the sea clutter data $u(n)$. Representative results of $\log_2 F_{(u)}(m)$ vs. $\log_2 m$ for the 14 range bins of one measurement are shown in Fig. 5(a), where the curves denoted by open circles are for data with the target, while the curves denoted by asterisks are for data without the target. We observe the curves are fairly linear in the range of $m = 2^4$ to about $m = 2^{12}$. They correspond to the time scale range of about 0.01 sec to 4 seconds, since the sampling frequency of the sea clutter data is 1000 Hz. Thus in this time scale range the sea clutter data can be classified as fractal. The H parameter of each curve is estimated by fitting a straight line to the $\log_2 F_{(u)}(m)$ vs. $\log_2 m$ curve in the range of $m = 2^4$ to $m = 2^{12}$. The estimated parameter is explicitly shown in Fig. 5(b). We notice that the H parameters of the curves for the data with the target are much larger than those for the data without the target. It turns out this is a generic feature for all the measurements.

What is the physical significance of the two time scales, one about 0.01 sec and the other around a few seconds, identified in FA? We observe that for time scale up to 0.01 sec, the amplitude waveform of sea clutter is fairly smooth, as can be evidently seen from Fig. 6. The time scale of a few seconds may correspond to how fast the wave pattern on the sea surface changes. These time scales may slightly vary with sea and weather conditions. Interestingly, these two time scales have been explicitly accounted for by the compound-Gaussian model [57], where the time scale of a few seconds is considered as the decorrelation time of the texture.

FA suggests that the sea clutter data is a type of $1/f^{\alpha}$ noise for the time scale range of around 0.01 sec to a few seconds. It is interesting to estimate the PSD of sea clutter data to check whether it indeed decays as a power-law in the frequency range corresponding to the time scale range identified, and if yes, to check whether the relation of $\alpha = 2H + 1$ holds.

We have systematically estimated the PSD from all the sea clutter data. Two representative PSD curves are shown in Fig. 7 in log-log scale. The dashed straight lines in Fig. 7 are in the frequency range of 1 to 100 Hz, which corresponds to the time scale range of around 0.01 sec to a few seconds. Those two straight lines are obtained by the least-squares fit to the PSD curves in that frequency range. The slopes are 1.14 and 1.72, which are equivalent to $H = 0.07$ and 0.36. The Hurst parameters for the same datasets estimated by FA are 0.07 and 0.37. Hence, FA and spectral analysis are very consistent. It is worth noting, though, that it is not easy to identify the scaling range by spectral analysis alone.

Next, let us examine if a robust detector for detecting targets within sea clutter can be developed based on H estimated in the time scale range of 0.01 sec to a few seconds identified. We have systematically studied 392 time series of the sea clutter data measured under various sea and weather conditions. To better appreciate the detection performance, we have first only focused on primary target bins, but omitted those secondary target bins, since sometimes it is hard to determine whether a secondary target bin really hits a target or not. After omitting those secondary target range bins, the histograms (equivalent to pdfs) for the H parameter under the two hypotheses (the bins without targets and those with primary targets) for HH and VV datasets are shown in Figs. 8(a, b), respectively. We observe that the histograms completely separate for the HH datasets. This means the detection accuracy can be 100%. The accuracy for the VV datasets is also very good, except for two measurements. Interestingly, those measurements correspond to the two HH measurements with the smallest H values. We suspect there might be some kind of experimental error in those two measurements.

Before proceeding, we make a comment. If one tries to estimate H from other intervals of time by using maximum likelihood estimation, then H fails to detect targets within sea clutter. This makes it clear that characterization of fractal scaling break is among the most important when

detecting patterns using fractal theory. This feature is particularly important in practice, since experimental data is finite, and therefore, may not confirm to ideal mathematical definition of fractal processes with long range correlations.

4.1.2 Analysis of the integrated data

Now we apply FA to the data $v(n)$ obtained by integrating $u(n)$. A typical result of $\log_2 F_{(v)}(m)$ vs. $\log_2 m$ is shown in Fig. 5(c) and the H values (estimated by fitting a straight line to $\log_2 F_{(v)}(m)$ vs. $\log_2 m$ in the range of $m = 2^4$ to $m = 2^{12}$) for the 14 range bins shown in Fig. 5(d). From Fig. 5(c), one would conclude that the data have excellent fractal scaling behavior. However, this is an illusion due to the large y-axis range in the figure. This point will be further discussed in Sec. 5. While the variation of H vs. the range-bin number still indicates which bins hit the target, overall, the H values are very close to 1. Because of this, FA-based fractal scaling analysis becomes ineffective for the purpose of distinguishing sea clutter data with and without targets. This can be readily seen from Figs. 8(c, d), where we observe that the histogram for the H parameters for the data without targets significantly overlaps with that for the data with primary targets for both HH and VV datasets.

Let us explain why FA may fail for detecting targets within sea clutter. This lies in the observation that the largest Hurst parameter given by FA is 1. To explain this idea, let us assume $y(n) \sim n^{\beta}, \beta > 1$. Then $\left\langle |y(n+m)-y(n)|^2 \right\rangle = \left\langle [(n+m)^{\beta} - n^{\beta}]^2 \right\rangle$ is dominated by the terms with large n. When this is the case, $(n+m)^{\beta} = [n(1+m/n)]^{\beta} \approx n^{\beta}[1+\beta m/n]$. One then sees that $\left\langle |y(n+m)-y(n)|^2 \right\rangle \sim m^2$, i.e., $H = 1$. We call this the saturation phenomenon associated with FA. An important implication of this discussion is that whenever one observes a Hurst parameter very close to 1, one has to be alerted that it may be advantageous to re-do the analysis by treating the original time series as a "random walk" process instead of an "increment" process. In other words, apply FA on the original data instead of the integrated data. It should be noted that one can similarly prove that H estimated by FA cannot be negative.

4.1.3 Analysis of the differenced data

We now apply FA to the data $w(n)$ obtained by differencing $u(n)$. A representative result of $\log_2 F_{(w)}(m)$ vs. $\log_2 m$ for one single measurement is shown in Fig. 5(e) and the variation of H vs. the range-bin number shown in Fig. 5(f). we observe that all the curves are almost flat in the range of about $m = 2^4$ to $m = 2^{16}$, thus the H values for the 14 range bins are all very close to 0. Since the difference between the H parameters for the range bins with and without the target is very small, FA-based fractal scaling analysis again becomes ineffective for the purpose of detecting targets within sea clutter data. This can be readily appreciated from Figs. 8(e, f), where we observe that for both HH and VV datasets, the histograms of the H parameters for the sea clutter data with and without targets significantly overlap.

4.1.4 Brief summary

It is evident from the above analyses that the sea clutter data should be treated as a random-walk-type process. Realizing this, one can then readily develop a method for detecting targets from sea clutter radar returns.

4.2 Detrended fluctuation analysis of sea clutter

Let us now discuss DFA of sea clutter. We also re-denote $F_d(m)$ in Eq. (10) by $F_{d(u)}(m)$, $F_{d(v)}(m)$, or $F_{d(w)}(m)$, depending on whether DFA is applied to the $u(n)$, $v(n)$, or $w(n)$ time series.

4.2.1 Analysis of original sea clutter data

Let us start with applying DFA to the original sea clutter amplitude data $u(n)$. We analyze the same measurement that has been studied by FA earlier. Representative results of $\log_2 F_{d(u)}(m)$ vs. $\log_2 m$ for the 14 range bins are shown in Fig. 9(a). We observe that the curves for data with and without the target are all very similar to those obtained by FA. We also identify the two time scales, one about 0.01 sec and the other around a few seconds. Again we notice that the H values for the data with the target are much larger than those for the data without the target. This is explicitly shown in Fig. 9(b). It turns out that this feature is also generically true for all the measurements.

Since the difference between the results given by DFA and FA is very minor when the original sea clutter data $u(n)$ is considered, we thus conclude that the sea clutter data does not contain any significant trends, especially linear.

Let us now carefully examine if the H parameter estimated by DFA can be developed into a robust target detector within sea clutter. We have also systematically studied 392 time series of the sea clutter data measured under various sea and weather conditions, by focusing on bins with primary targets. The histograms for H under each hypothesis (the bins without targets and those with primary targets) for HH and VV datasets are shown in Figs. 10(a, b), respectively. We observe that the detection accuracy for both HH and VV datasets is very high, except for two measurements. Interestingly, those measurements correspond to the two measurements where FA works on the HH but fails in the VV measurements.

4.2.2 Analysis of the integrated data

Let us now apply DFA to the data $v(n)$ obtained by integrating $u(n)$. Fig. 9(c) shows a representative example of $\log_2 F_{d(v)}(m)$ vs. $\log_2 m$ for one single measurement, where the curves denoted by open circles are for data with the target, while the curves denoted by asterisks are for data without the target. As will be discussed in Sec. 5, the seemingly good fractal scaling behavior is also an illusion. The H value for each curve is estimated by fitting a straight line to $\log_2 F_{d(v)}(m)$ vs. $\log_2 m$ in the range of $m = 2^4$ to $m = 2^{12}$. The variation of H vs. the range-bin number for the 14 range bins is shown in Fig. 9(d). We observe that the H value can be used for separating sea clutter data with and without the target.

Comparing Figs. 9(b) and (d), one notices that the H values estimated from $u(n)$ and $v(n)$ time series differ by around 1. How may we understand this feature? Notice that when the process $u(n)$ has a PSD of the form $1/f^{\alpha}$, where $\alpha = 2H+1,\ 0 < H < 1$, then the integrated process $v(n)$ has a PSD of the form $1/f^{\alpha+2}$. If we still have $\alpha+2 = 2H^*+1$, then $H^* = H+1$. Therefore, when DFA is used, the relation of $\alpha = 2H+1$ [52] holds regardless of whether H being larger than 1 or not. We thus have an interesting observation that DFA can overcome the saturation problem associated with FA.

We have also examined the performance of target detection within 392 time series of the sea clutter data measured under various sea and weather conditions. Our analysis shows that this method is very effective for distinguishing sea clutter data with and without targets. This can be evidently seen from Fig. 10(c), where we observe that the histograms of H for the sea clutter data with and without targets for HH datasets are completely separated. In fact, the separation is larger than that revealed by FA. The detection accuracy for VV datasets is also very good, except for two measurements, as shown in Fig. 10(d). Again, those VV measurements correspond to the two VV measurements where FA is not very effective either.

It is worth pointing out that if one tries to estimate H from other intervals of time, then DFA fails to detect targets within sea clutter, either $u(n)$ or $v(n)$ data. This very fact again shows that fractal scaling break is at least as important as fractal scaling behavior for pattern recognition purposes.

4.2.3 Analysis of the differenced data

Finally, we apply DFA to the data $w(n)$ obtained by differencing $u(n)$. A representative result of $\log_2 F_{(w)}(m)$ vs. $\log_2 m$ for one single measurement is shown in Fig. 9(e) and the variation of H vs. the range-bin number shown in Fig. 9(f). Similar to the results obtained by applying FA to the $w(n)$ time series, we observe from Fig. 9(e) that the curves for the sea clutter data with and without the target are all flat in the range of $m = 2^4$ to $m = 2^{16}$, thus the H values for the 14 range bins are all very close to 0, and this is explicitly shown in Fig. 9(f). Since the difference between the H values for the sea clutter data with and without the target is very minor, DFA-based fractal scaling analysis fails for the purpose of distinguishing sea clutter data with targets from those without targets. This can be readily seen from Figs. 10(e, f), where the histograms for the H parameter under the two hypotheses (the range bins without targets and those with primary targets) for HH and VV datasets are shown respectively. We observe that the histogram for the data with primary targets significantly overlaps with that for the data without targets. The reason is of course that all the H values are very close to 0.

4.2.4 Brief summary

Our DFA of sea clutter clearly indicates that two robust detectors, with accuracy close to 100%, can be readily developed by applying DFA to the original data and the integrated data.

4.3 Wavelet-based fractal scaling analysis of sea clutter

Let us now apply the wavelet-based fractal scaling analysis to the three types of data, the original sea clutter data $u(n)$, the data $v(n)$ obtained by integrating $u(n)$ and the data $w(n)$ obtained by differencing $u(n)$. Again, for notational clarity, we re-denote $\Gamma(j)$ by $\Gamma_{(u)}(j)$, $\Gamma_{(v)}(j)$, or $\Gamma_{(w)}(j)$, depending on whether the wavelet-based fractal scaling analysis is applied to the $u(n)$, $v(n)$, or $w(n)$ time series. Representative results for $\log_2 \Gamma(j)$ vs. j curves for the three types of data are shown in Figs. 11(a, c, e), while the H values for the three types of data are shown in Figs. 11(b, d, f), respectively. For the purpose of comparing with FA and DFA, we focus on the time scale range from about 0.01 sec to a few seconds. It is obvious from Figs. 11(b, d, f) that the H values estimated by the wavelet-based fractal scaling analysis can separate the sea clutter data with and without targets very well, no matter which type of data is considered.

Let us now understand the meanings of these computations. We have noted that the H value estimated by applying the wavelet-based fractal scaling analysis to the increment process $w(n)$ should be consistent with that obtained by applying either FA or DFA to the random-walk-type process $u(n)$. Comparing Fig. 11(f) with Fig. 5(b) and Fig. 9(b), we see that this is indeed the case, except an interesting feature from the wavelet-based method: the estimated H values can be negative. This feature can be viewed as an improvement of the wavelet-based method over both FA and DFA: the H values estimated by the latter two methods have to be non-negative, regardless of the process under investigation.

Interestingly, the H parameters calculated from $v(n)$, $u(n)$ and $w(n)$ time series differ by around 1 in turn. This is understandable, noticing that $v(n)$ is the "random walk" process of $u(n)$, while $u(n)$ is the "random walk" process of $w(n)$. When the process $u(n)$ has a power-law PSD of the form $1/f^{\alpha}$, this means the PSD for $w(n)$ and $v(n)$ has the form $1/f^{\alpha-2}$ and $1/f^{\alpha+2}$, respectively. The fact that the estimated H differs by around 1 indicates that the relation of $\alpha = 2H + 1$ holds

without any constraint on the admissible range of α or H.

Finally, we examine the performance of target detection within 392 time series of the sea clutter data measured under various sea and weather conditions. The results are summarized in Figs. 12(a-f). Since the histograms of the H parameter for the sea clutter data with and without targets for HH datasets are completely separated, we conclude that the wavelet-based fractal scaling analysis is very effective in detecting targets within sea clutter data, regardless of which process is analyzed. The detection accuracy for VV datasets is also very good, except for two measurements, as shown in Figs. 12(b, d, f).

It is interesting to make comparisons about the performance of target detection by applying FA to $u(n)$, DFA to $u(n)$, and the wavelet-based fractal scaling analysis to the $w(n)$ data. By comparing Figs. 8(a, b), 10(a, b) and 12(e, f), we observe that the sea clutter data with and without targets can be best separated by the wavelet-based approach, especially for the HH datasets, since the gap between the histograms of H for the range bins with primary targets and those without targets is the biggest. The detection accuracy of the FA-based fractal scaling analysis is also as high as 100%, since the histograms for the sea clutter data with and without targets are completely separated for the HH datasets. The detection performance of the DFA-based fractal scaling analysis is also very good, except for two measurements.

Why does the wavelet-based approach give the best detection performance? This is because the H values estimated by the wavelet-based approach can be negative, while those estimated by both FA and DFA have to be non-negative. Thus the difference between H values for the sea clutter data with and without targets is best represented by the wavelet-based approach.

We also compare the performance of target detection by applying DFA to $v(n)$ and the wavelet-based approach to $u(n)$. By comparing Figs. 10(c,d) with 12(a,b), we observe that the detection performance is very similar for the two methods (the wavelet-based approach is slightly better).

5 Conclusion and Discussions

In this paper, we have examined three types of fractal scaling analyses, FA, DFA, and the wavelet-based, for detecting small low observable targets within sea clutter. We have applied these methods

to analyze three types of data, the measured sea clutter amplitude data $u(n)$, the data $v(n)$ obtained by integrating $u(n)$, and the data $w(n)$ obtained by differencing $u(n)$. We find that sea clutter data exhibit fractal behaviors in the time scale range of about 0.01 sec to around a few seconds. By systematically studying 392 sea clutter time series measured under various sea and weather conditions, we find very effective methods for detecting targets within sea clutter by applying FA to $u(n)$, DFA to both $u(n)$ and $v(n)$, and the wavelet-based approach to all three types of data. Based on the limited data available to us, the accuracy of these detectors is found to be close to 100%.

We emphasize that the fractal scaling behavior identified from sea clutter data is only valid within the time scale range of about 0.01 sec and a few seconds. By applying FA or DFA to $u(n)$, and the wavelet-based approach to both $u(n)$ and $w(n)$, one can readily identify these two time scales. When applying the three methods to $v(n)$ (Figs. 5(c), 9(c) and 11(c)), one might think that sea clutter data have excellent fractal scaling behavior over the entire range of time. However, this is an illusion due to the large y-axis range in the figures. To better see this, as an example, we reduce the y-axis range by plotting $\log_2[F_{d(v)}(m)/m]$ vs. $\log_2 m$, as shown in Fig. 13 (corresponding to Fig. 9(c)). Now it is clear that the curves for sea clutter data without target change abruptly around $m = 2^4$ nd $m = 2^{12}$, which correspond to the time scale range of about 0.01 sec and 4 seconds. We have pointed out that the two time scales have specific physical meanings: below 0.01 sec, the data is fairly smooth, hence cannot be fractal; above a few seconds, the wave pattern on the sea surface may change, hence, the data may change to a different behavior (possibly another type of fractal). With the available length of the data (about 2 min), the latter cannot be resolved, however. It is possible that these time scales may slightly change with sea and weather conditions.

We have mentioned that if one tries to estimate H from other intervals of time, then H fails to detect targets within sea clutter. This very fact makes it clear that fractal scaling break is at least as important as fractal scaling behavior for pattern recognition purposes. This feature is particularly important in practice, since experimental data is finite, and therefore, may not confirm to ideal mathematical definition of fractal processes with long range correlations.

To facilitate application of these methods in practice, we emphasize that FA gives $0 \leq H \leq 1$,

DFA gives $0 \leq H$, while the wavelet-based method gives an estimated H that can not only be larger than 1, but also be negative. Therefore, the wavelet-based method appears the easiest to use in practice. Finally, readers interested in these methods are strongly encouraged to contact with the authors to obtain the codes.

References

[1] F.A. Fay, J. Clarke, and R. S. Peters, “Weibull distribution applied to sea-clutter”, *Proc. IEE Conf. Radar’77*, London, U.K., pp. 101-103, 1977.

[2] F.E. Nathanson, *Radar design principles* (McGraw Hill), pp. 254-256, 1969.

[3] G.V. Trunk, S.F. George, “Detection of targets in non-Gaussian sea clutter”, *IEEE Tran. Aero. Elec. Sys.* 6, pp. 620-628, 1970.

[4] H.C. Chan, “Radar sea-clutter at low grazing angles”, *Proc. Inst. Elect. Eng.* **F137**, 102-112 (1990).

[5] E. Jakeman and P.N. Pusey, “A model for non Rayleigh sea echo”, *IEEE Trans Antennas & Propagation*, vol. 24. pp. 806-814, 1976.

[6] K. D. Ward, C. J. Baker, and S. Watts, “Maritime surveillance radar Part 1: Radar scattering from the ocean surface”, *Proc. Inst. Elect. Eng.* **F137**, 51-62 (1990).

[7] T. Nohara and S. Haykin, “Canadian East Coast radar trials and the *K*-distribution”, *Proc. Inst. Elect. Eng.* **F138**, 80-88 (1991).

[8] F. Gini, “Performance Analysis of Two Structured Covariance Matrix Estimators in Compound-Gaussian Clutter”, *Signal Processing* **80**, 365-371 (2000).

[9] F.L. Posner, “Spiky sea clutter at high range resolutions and very low grazing angles”, *IEEE Tran. Aero. Elec. Sys.* **38**, pp. 58-73, 2002.

[10] S. Sayama and M. Sekine, “Log-normal, log-Weibull and K-distributed sea clutter”, *IEICE Trans. Commun.* **E85-B**, 1375-1381 (2002).

[11] A.I. Morrison and M.A. Srokosz, “Estimating the fractal dimension of the sea-surface - a 1st attempt”, *Annales Geophysicae-Atmospheres HYdrospheres and Space Sci.* **11**, 648-658 (1993).

[12] M. Martorella, F. Berizzi, E.D. Mese, “On the fractal dimension of sea surface backscattered signal at low grazing angle IEEE”, *IEEE Trans. Antennas & Propagation* **52**, 1193-1204 (2004).

[13] G. Franceschetti, A. Iodice, M. Migliaccio, D. Riccio, “Scattering from natural rough surfaces modeled by fractional Brownian motion two-dimensional processes”, *IEEE Trans. Antennas & Propagation* **47**, 1405-1415 (1999).

[14] S. Haykin and S. Puthusserypady, “Chaotic dynamics of sea clutter”. *Chaos*, **7**, 777-802 (1997).

[15] S. Haykin, *Chaotic dynamics of sea clutter* (John Wiley) 1999.

[16] S. Haykin, R. Bakker, and B.W. Currie, “Uncovering nonlinear dynamics-the case study of sea clutter”, *Proc. IEEE* **90**, 860-881 (2002).

[17] M.R. Cowper and B. Mulgrew, “Nonlinear Processing of High Resolution Radar Sea Clutter,” *Proc. IJCNN* **4**, pp. 2633-2638 (1999).

[18] M. Davies, “Looking for Non-Linearities in Sea Clutter,” *IEE Radar and Sonar Signal Processing*, Peebles, Scotland, July 1998.

[19] J.B. Gao and K. Yao, “Multifractal features of sea clutter”, *IEEE Radar Conference 2002*, Long Beach, CA, April, 2002.

[20] J.B. Gao, S.K. Hwang, H.F. Chen, Z. Kang, K. Yao, and J.M. Liu, “Can sea clutter and indoor radio propagation be modeled as strange attractors?” *The 7th Experimental Chaos Conference*, San Diego, USA, August pp. 25-29, 2002.

[21] M. McDonald and A. Damini, “Limitations of nonlinear chaotic dynamics in predicting sea clutter returns”, *IEE Proc-Radar Son Nav*, vol. 151. pp. 105-113, 2004.

[22] T. Thayaparan, S. Kennedy, “Detection of a manoeuvring air target in sea-clutter using joint time-frequency analysis techniques”, *IEE Proceedings-Radar, Sonar and Navigation* **151** 19-30 (2004).

[23] G. Davidson and H.D. Griffiths, “Wavelet detection scheme for small targets in sea clutter”, *Electronics Lett.*, vol. 38. pp. 1128-1130, 2002.

[24] T. Bhattacharya and S. Haykin, “Neural Network-based Radar Detection for an Ocean Environment”, *IEEE Trans. Aerospace and Electronic Systems* **33** 408-420 (1997).

[25] H. Leung, N. Dubash, and N. Xie, “Detection of small objects in clutter using a GA-RBF neural network”, *IEEE Tran. Aero. Elec. Sys.*, vol. 38. pp. 98-118, 2002.

[26] N. Xie, H. Leung, and H. Chan, “A multiple-model prediction approach for sea clutter modeling”, *IEEE Tran. Geosci Remote*, vol. 41. pp. 1491-1502, 2003.

[27] C.P. Lin, M. Sano, S. Sayama, and M. Sekine, “Detection of radar targets embedded in sea ice and sea clutter using fractals, wavelets, and neural networks”, *IEICE Trans. Commun.*, vol. E83B. pp. 1916-1929, 2000.

[28] T. Lo, H. Leung, J. Litva and S. Haykin, “Fractal characterisation of sea-scattered signals and detection of sea-surface targets”, *IEE Proc.*, vol. F140. pp. 243-250, 1993.

[29] C.-P. Lin, M. Sano, and M. Sekine, “Detection of radar targets by means of fractal error”, *IEICE Trans. Commun.*, vol. E80-B. pp. 1741-1748, 1997.

[30] B.E. Cooper, D.L. Chenoweth, and J.E. Selvage, “Fractal error for detecting man-made features in aerial images”, *Electronics Letters*, vol. 30. pp. 554-555, 1994.

[31] D. Gan, Z. Shouhong, “Detection of sea-surface radar targets based on multifractal analysis”, *Electronics Letters* **36**, 1144-1145 (2000).

[32] J. Hu, W.W. Tung, and J.B. Gao, "Detection of low observable targets within sea clutter by structure function based multifractal analysis", *IEEE Trans. Antennas & Propagation* **54**, 135-143 (2006).

[33] D.C. Kim, S. Sayama, M. Sekine, "Detection of target embedded in sea clutter by means of millimeter wave radar", *International Journal of Infrared and Millimeter Waves* **24**, 1499-1508 (2003).

[34] B.B. Mandelbrot, *The Fractal Geometry of Nature* (San Francisco: Freeman, 1982).

[35] W.H. Press, "Flicker noises in astronomy and elsewhere", *Comments on Astrophysics*, vol. 7. pp. 103-119, 1978.

[36] P. Bak, *How Nature Works: the Science of Self-Organized Criticality* (Copernicus, 1996).

[37] G.M. Wornell, *Signal processing with fractals : a wavelet-based approach* (Prentice Hall, 1996).

[38] W.E. Leland, M.S. Taqqu, W. Willinger, and D.V. Wilson, "On the self-similar nature of Ethernet traffic (extended version)", *IEEE/ACM Trans. on Networking*, Vol. 2, 1-15 (1994).

[39] J. Beran, R. Sherman, M.S. Taqqu, and W. Willinger, "Long-range-dependence in variable-bit-rate video traffic", *IEEE Trans. on Commun.*, **43** 1566-1579 (1995).

[40] V. Paxson and S. Floyd, "Wide Area Traffic—-The failure of Poisson modeling", *IEEE/ACM Trans. on Networking*, **3** 226-244 (1995).

[41] W. Li and K. Kaneko, "Long-Range Correlation and Partial 1/f α Spectrum in a Non-Coding DNA Sequence", *Europhys. Lett.* **17** 655-660 (1992).

[42] R. Voss, "Evolution of long-range fractal correlations and 1/f noise in DNA base sequences", *Phys. Rev. Lett.* **68** 3805-3808 (1992).

[43] C.-K. Peng, S.V. Buldyrev, A.L. Goldberger, S. Havlin, F. Sciortino, M. Simons and H.E. Stanley, "Long-Range Correlations in Nucleotide Sequences", *Nature* **356** 168-171 (1992).

[44] D. L. Gilden, T. Thornton, and M. W. Mallon, “1/f noise in human cognition”, *Science* **267** 1837-1839 (1995).

[45] J.B. Gao, V.A. Billock, I. Merk, W.W. Tung, K.D. White, J.G. Harris, and V.P. Roychowdhury, “Inertia and memory in ambiguous visual perception”, *Cognitive Processing* **7** 105-112 (2006).

[46] Y. Chen, M. Ding, and J. A. S. Kelso, “Long Memory Processes (1/f alpha Type) in Human Coordination”, *Phys. Rev. Lett.* **79** 4501-4504 (1997).

[47] J.J. Collins and C.J. De Luca, “Random Walking during Quiet Standing”, *Phys. Rev. Lett.* **73**, 764-767 (1994).

[48] V.A. Billock, “Neural acclimation to 1/f spatial frequency spectra in natural images transduced by the human visual system”, *Physica D* **137**, 379-391 (2000).

[49] V.A. Billock, G.C. de Guzman, and J.A.S. Kelso, “Fractal time and 1/f spectra in dynamic images and human vision”, *Physica D* **148**, 136-146 (2001).

[50] M. Wolf, “1//f noise in the distribution of primes”, *Physica A* **241** 493-499 (1997).

[51] J.B. Gao, Yinhe Cao, and Jae-Min Lee, “Principal Component Analysis of $1/f^{\alpha}$ Noise”, *Phys. Lett. A*, vol. 314. pp. 392-400, 2003.

[52] P. Talkner and R.O. Weber, “Power spectrum and detrended fluctuation analysis: Application to daily temperatures”, *Phys. Rev. E*, **62**, 150-160 (2000).

[53] J.B. Gao, J. Hu, W.W. Tung, Y.H. Cao, N. Sarshar, and V.P. Roychowdhury, “Assessment of long range correlation in time series: How to avoid pitfalls”, *Phys. Rev. E*, **73**, 016117 (2006).

[54] C.-K. Peng, S.V. Buldyrev, S. Havlin, M. Simons, H.E. Stanley, and A.L. Goldberger, “Mosaic organization of DNA nucleotides” *Phys. Rev. E* **49**, 1685-1689 (1994).

[55] K. Hu, P.C. Ivanov, Z. Chen, P. Carpena, and H.E. Stanley, “Effect of trends on detrended fluctuation analysis”, *Phys. Rev. E* **64**, 011114 (2001).

[56] G. Strang and T. Nguyen. 1997. Wavelet and filter banks. Wellesley-Cambridge Press, New York.

[57] A. Farina, F. Gini, M.V. Greco and L. Verrazzani, “High resolution sea clutter data: statistical analysis of recorded live data”, *IEE Proc.-Radar, Sonar Navig.*, **144**, 121-130 (1997).

Figure Captions

Fig. 1: Examples of the sea clutter amplitude data (a) without and (b) with target.

Fig. 2: Pyramidal structure of the output of wavelet multiresolution analysis.

Fig. 3: The scaling function $\phi_0(n)$ and the mother wavelet $\psi_0(n)$ of the Haar wavelet.

Fig. 4: (a) The input signal $x(n)$, (b,d,f) and (c,e,g) are the signal approximations and the signal details at resolution levels 1 through 3, respectively. $x(n) = SA_1 + SD_1 = SA_2 + SD_2 + SD_1 = SA_3 + SD_3 + SD_2 + SD_1$.

Fig. 5: The left column (a,c,e) shows the results by FA ($\log_2 F(m)$ vs. $\log_2 m$) for the 14 range bins for the original sea clutter data $u(n)$, the integrated data $v(n)$, and the differenced data $w(n)$, respectively. The corresponding H values are shown in (b,d,f). Open circles denote bins with target, while * denote bins without target. This rule applies to all other figures.

Fig. 6: Two short segments of the sea clutter amplitude data.

Fig. 7: (a) and (b) show the PSD of the two sea clutter data shown in Figs. 1(a) and (b), respectively.

Fig. 8: The left column (a,c,e) shows the results by FA (histograms of the bins without targets and those with primary targets of HH datasets) for $u(n)$, $v(n)$ and $w(n)$, respectively. The histograms of VV datasets are shown in (b,d,f). Open boxes denote the range bins without targets, while solid black boxes denote the bins with primary targets. This rule applies to all other figures.

Fig. 9: The left column (a,c,e) shows the results by DFA ($\log_2 F(m)$ vs. $\log_2 m$) for the 14 range bins for $u(n)$, $v(n)$ and $w(n)$, respectively. The corresponding H values are shown in (b,d,f).

Fig. 10: The left column (a,c,e) shows the results by DFA (histograms of the bins without and with targets for HH datasets) for $u(n)$, $v(n)$ and $w(n)$, respectively. The histograms for VV datasets are shown in (b,d,f).

Fig. 11: The left column (a,c,e) shows the results by the wavelet-based fractal scaling analysis ($\log_2 F(m)$ vs. $\log_2 m$) for the 14 range bins for $u(n)$, $v(n)$ and $w(n)$, respectively. The corresponding H values are shown in (b,d,f).

Fig. 12: The left column (a,c,e) shows the results by the wavelet-based fractal scaling analysis (histograms of the bins without and with targets for HH datasets) for $u(n)$, $v(n)$ and $w(n)$, respectively. The histograms for VV datasets are shown in (b,d,f).

Fig. 13: The $\log_2[F_{d(v)}(m)/m]$ vs. $\log_2 m$ curves for the 14 range bins for $v(n)$ using DFA.

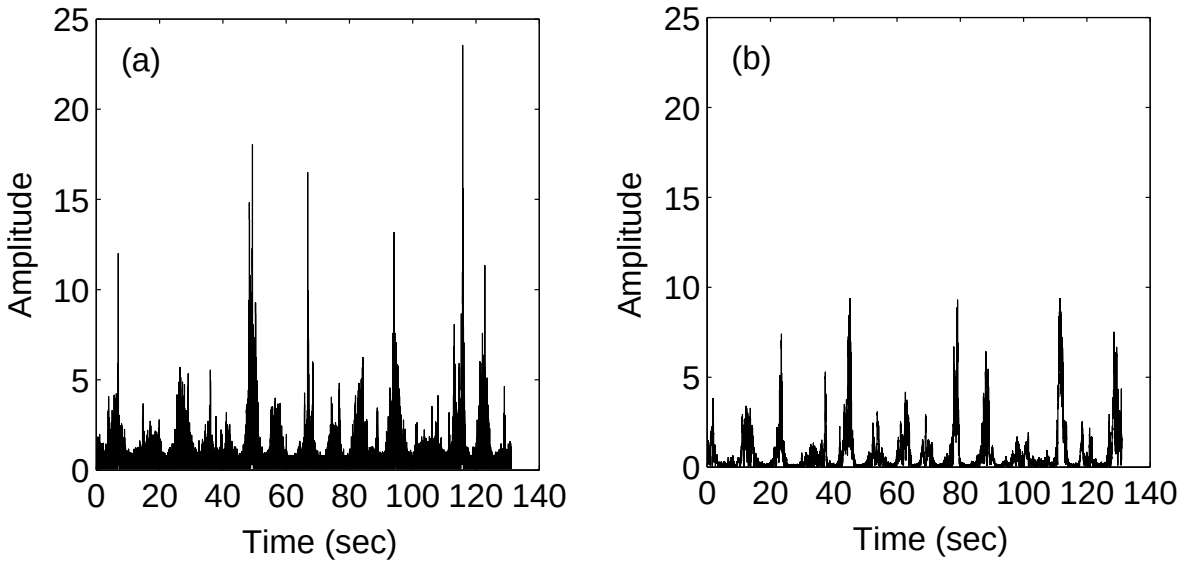

Figure 1:

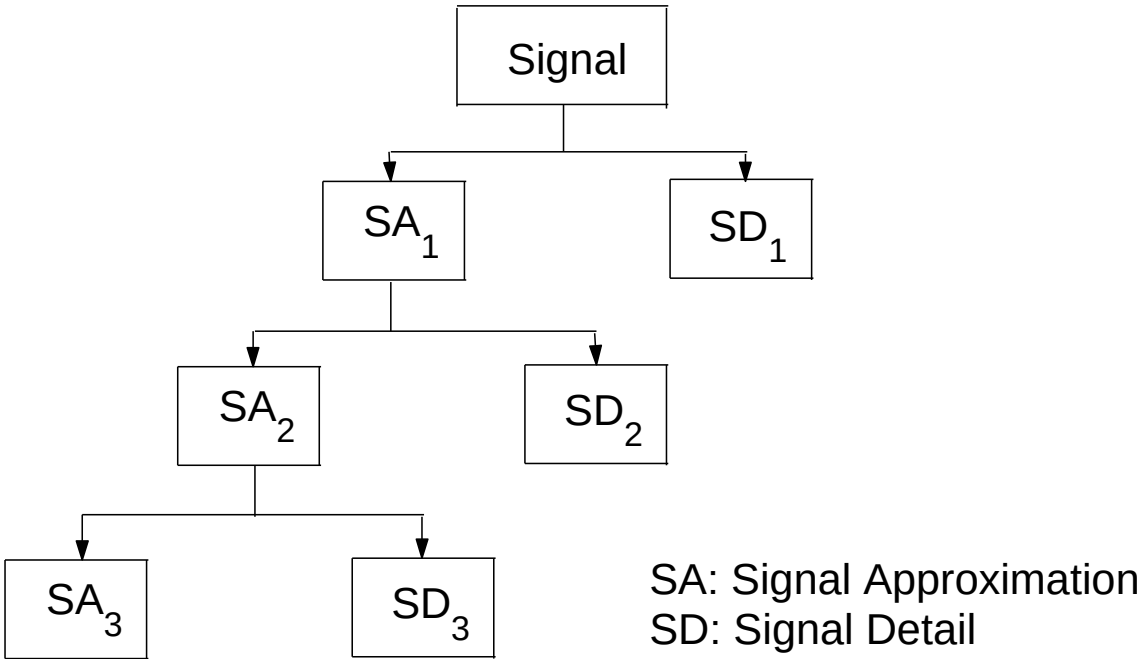
Signal
SA1
SD1
SA2
SD2
SA3
SD3
SA: Signal Approximation
SD: Signal Detail

Figure 2:

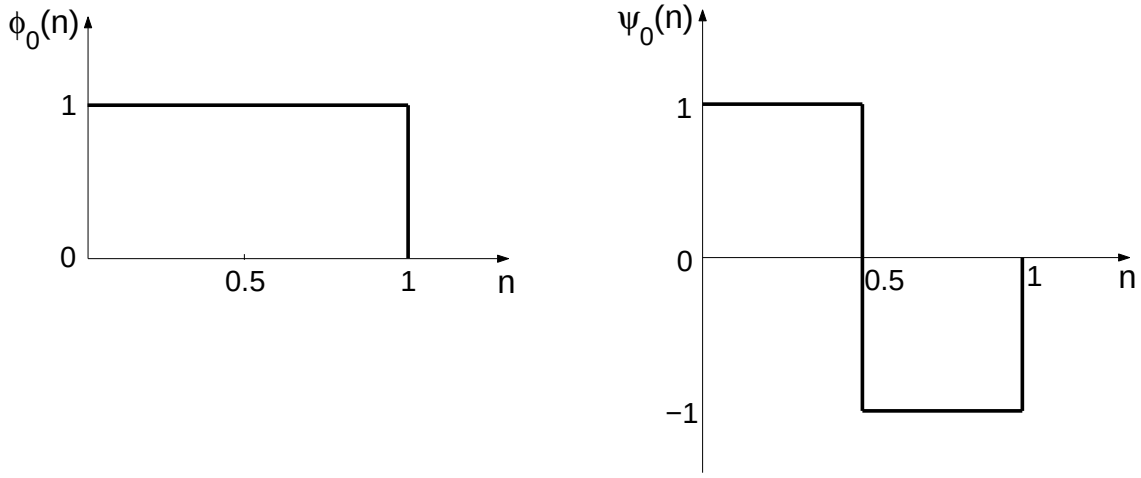

Figure 3:

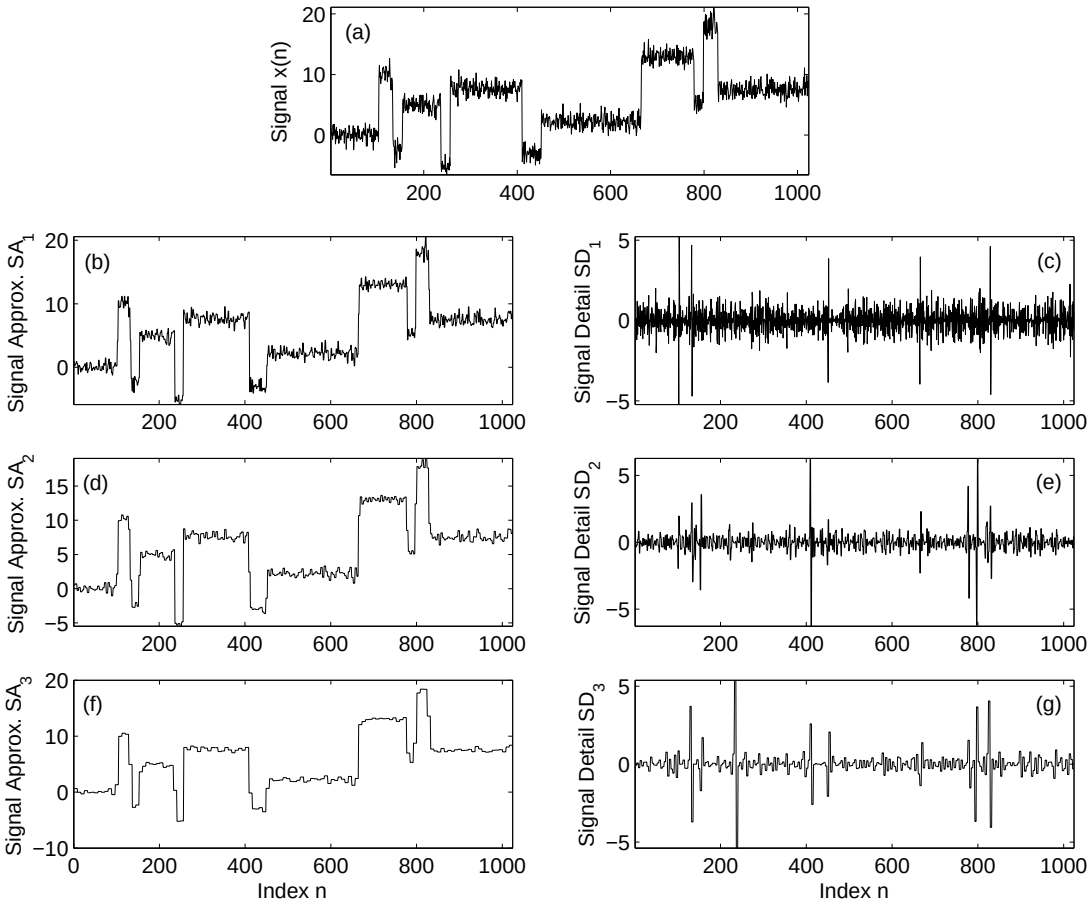
(a)
Signal x(n)
(b)
Signal Approx. SA1
(c)
Signal Detail SD1
(d)
Signal Approx. SA2
(e)
Signal Detail SD2
(f)
Signal Approx. SA3
(g)
Signal Detail SD3
Index n
Index n

Figure 4:

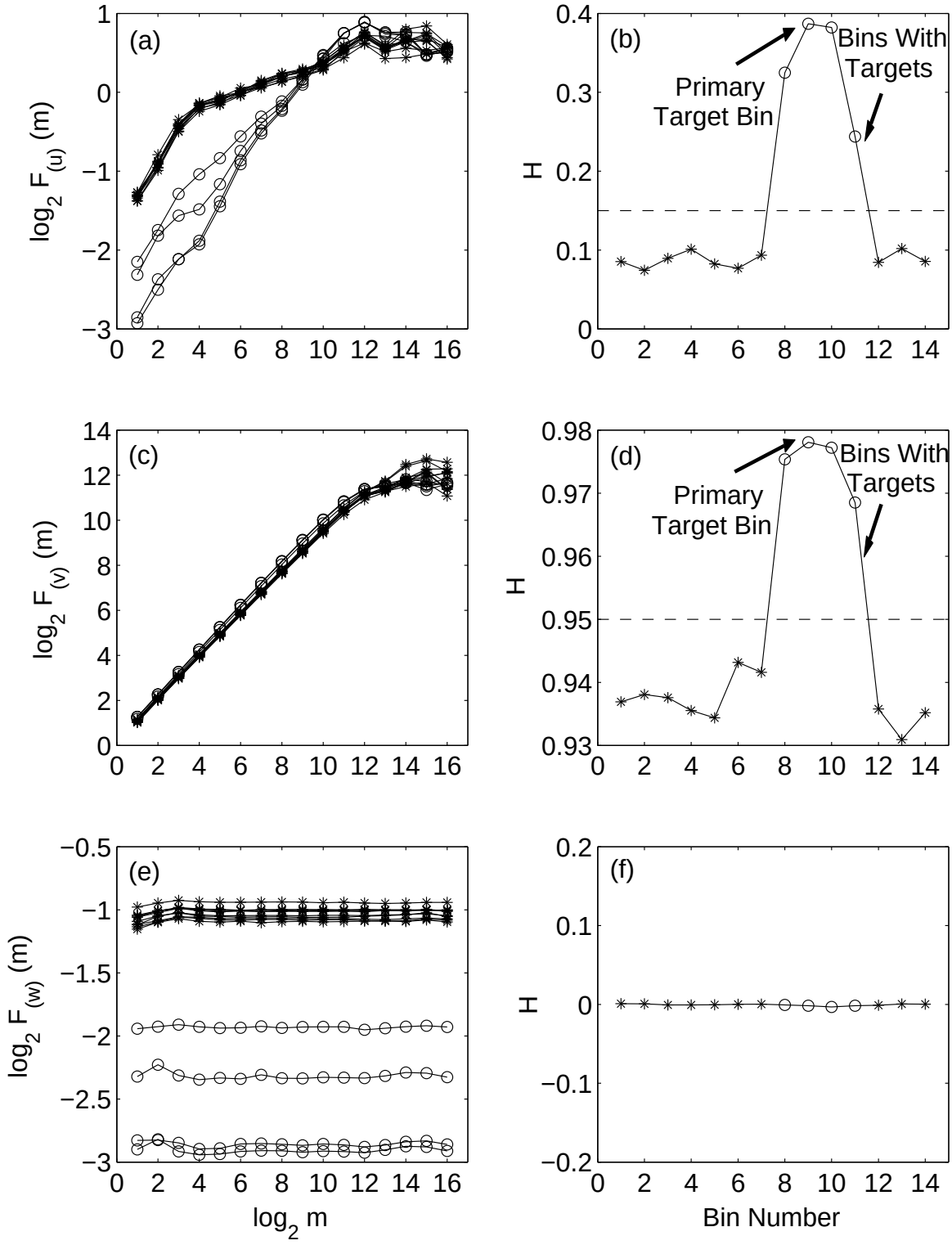
(a)
(b)
(c)
(d)
(e)
(f)
Primary
Target Bin
Bins With
Targets
log2 F(u) (m)
log2 F(v) (m)
log2 F(w) (m)
H
log2 m
Bin Number

Figure 5:

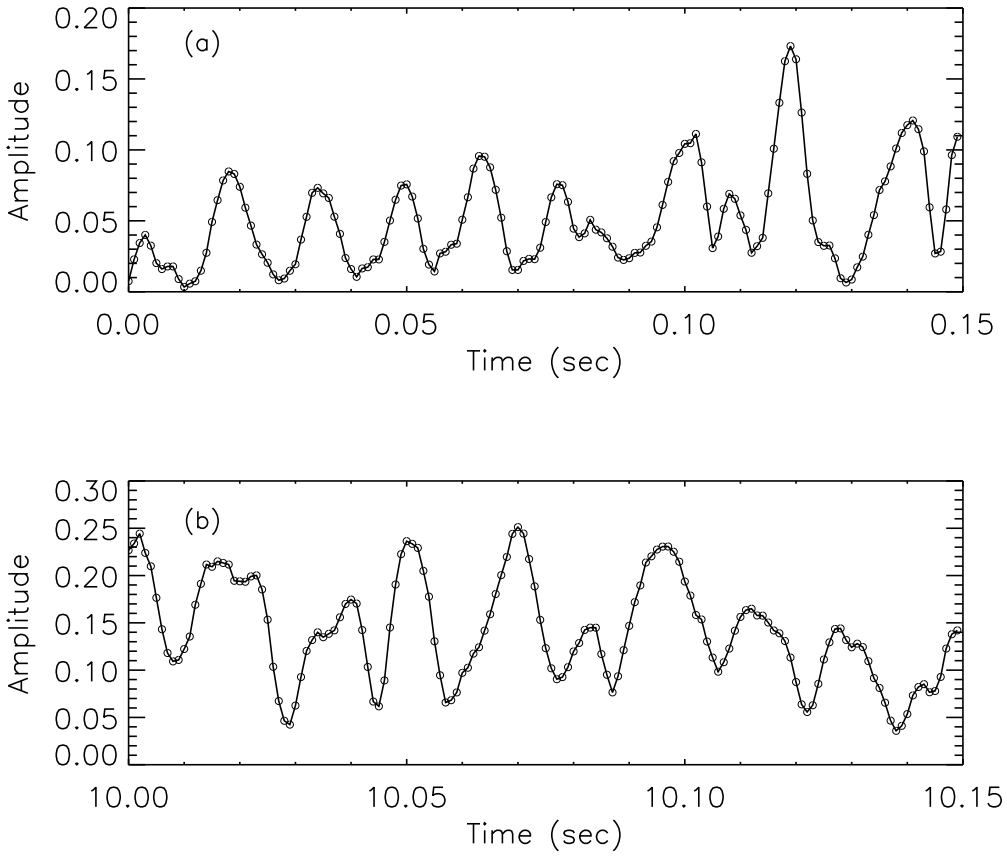
(a)
Amplitude
0.20
0.15
0.10
0.05
0.00
0.00
0.05
0.10
0.15
Time (sec)
(b)
Amplitude
0.30
0.25
0.20
0.15
0.10
0.05
0.00
10.00
10.05
10.10
10.15
Time (sec)

Figure 6:

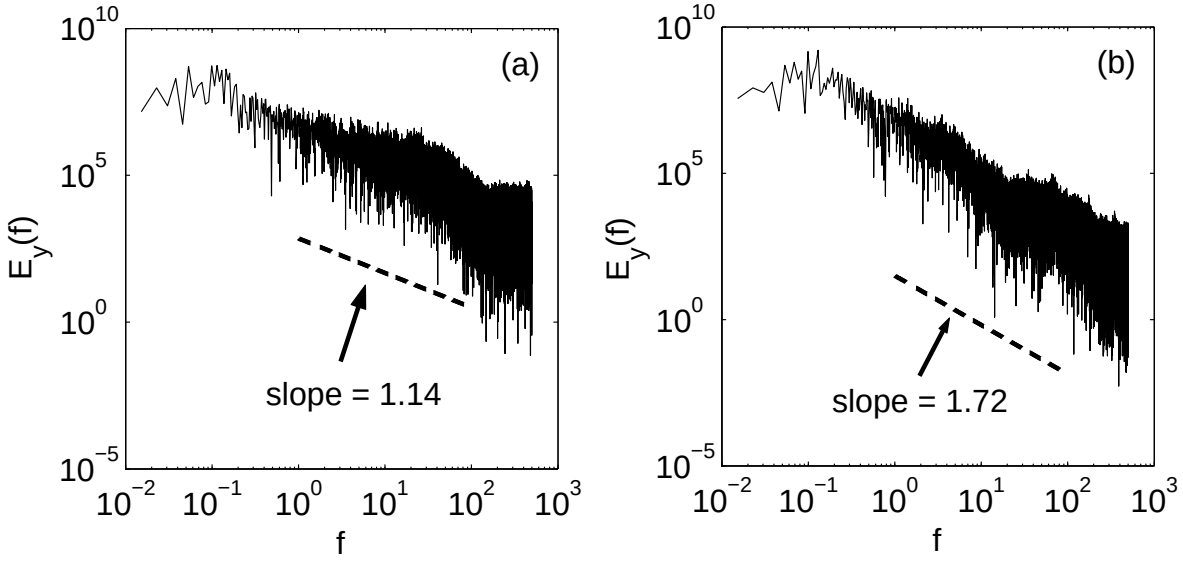

Figure 7:

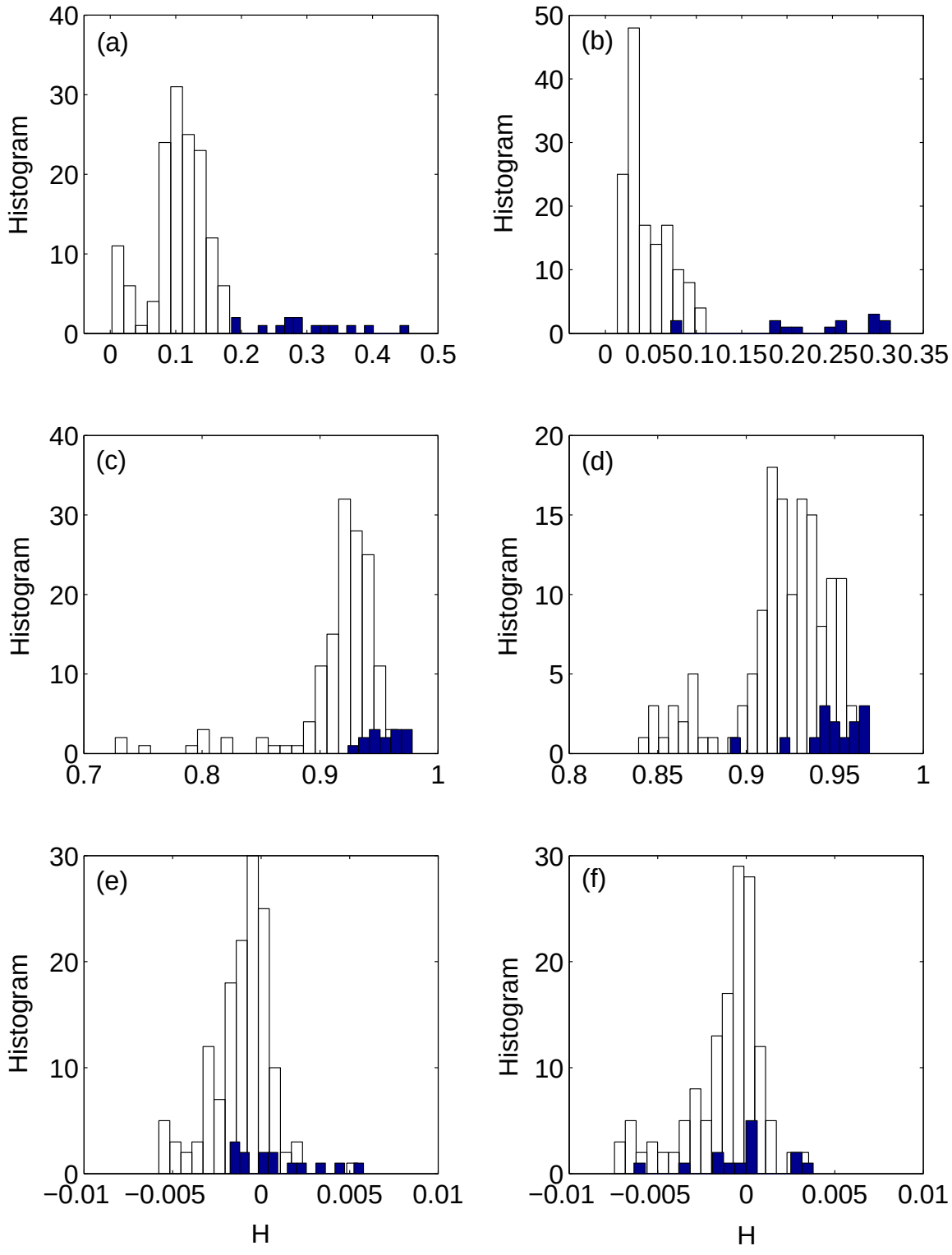

Figure 8:

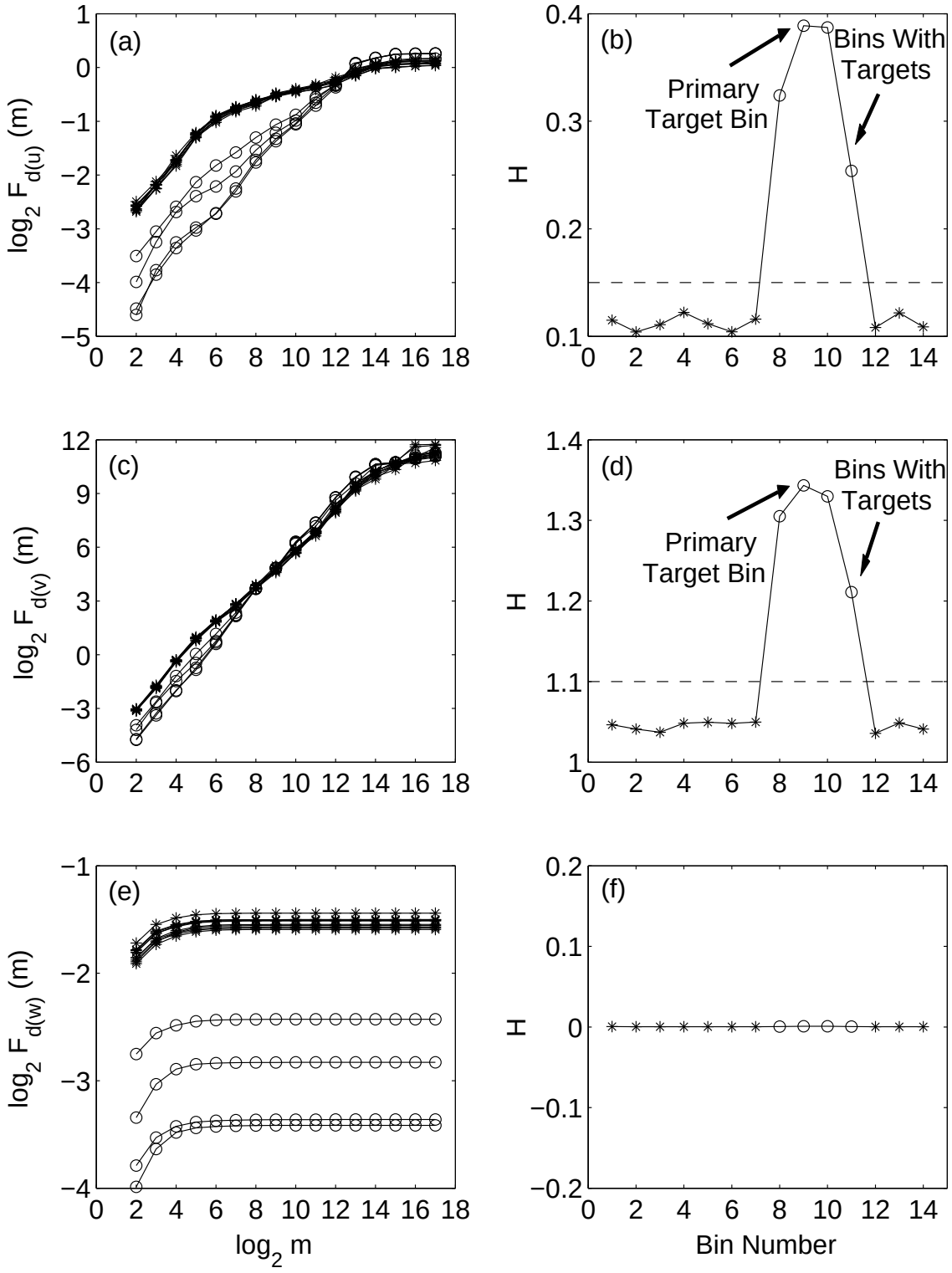
(a)
(b)
(c)
(d)
(e)
(f)
Primary
Target Bin
Bins With
Targets
log2 F d(u) (m)
log2 F d(v) (m)
log2 F d(w) (m)
H
log2 m
Bin Number

Figure 9:

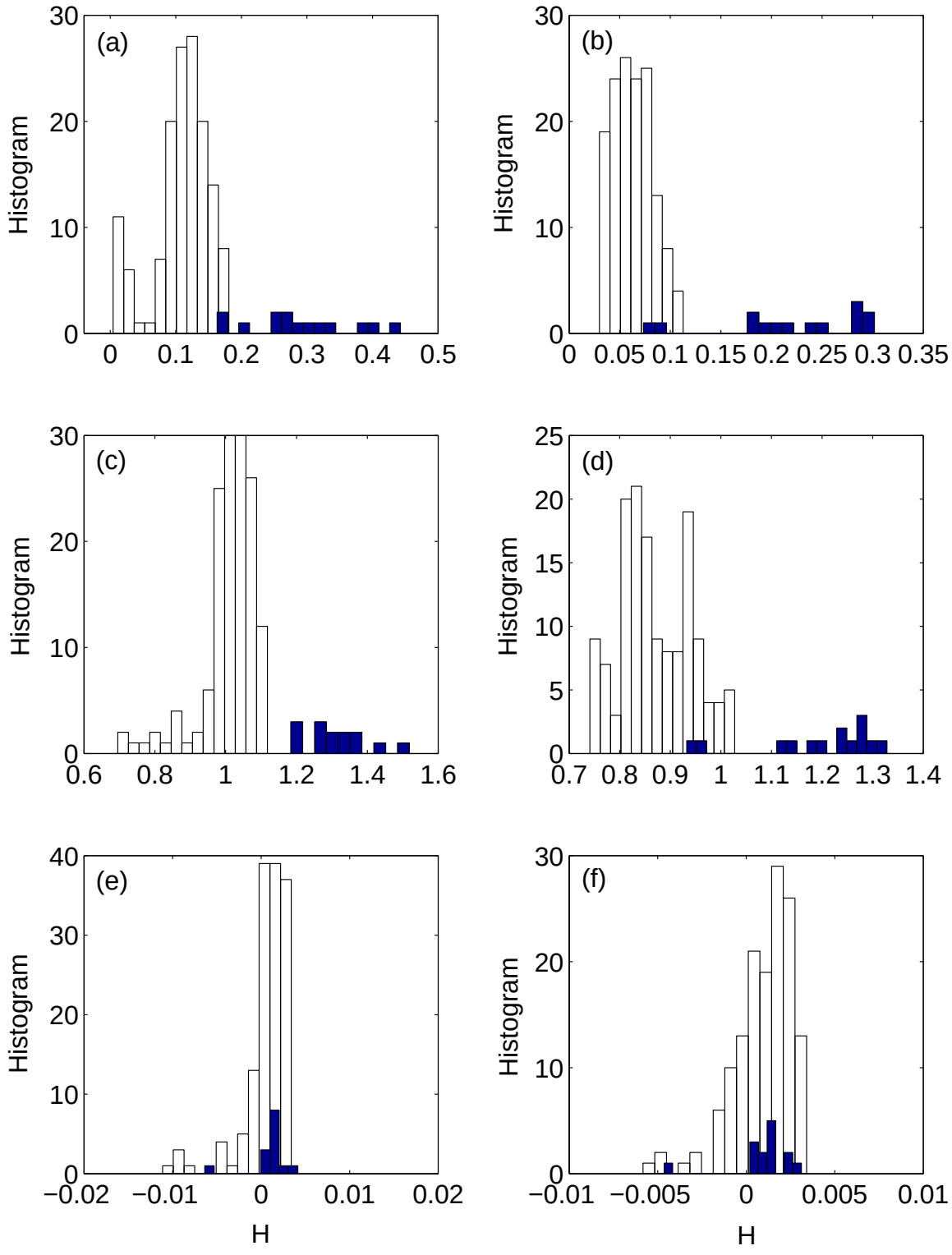

Figure 10:

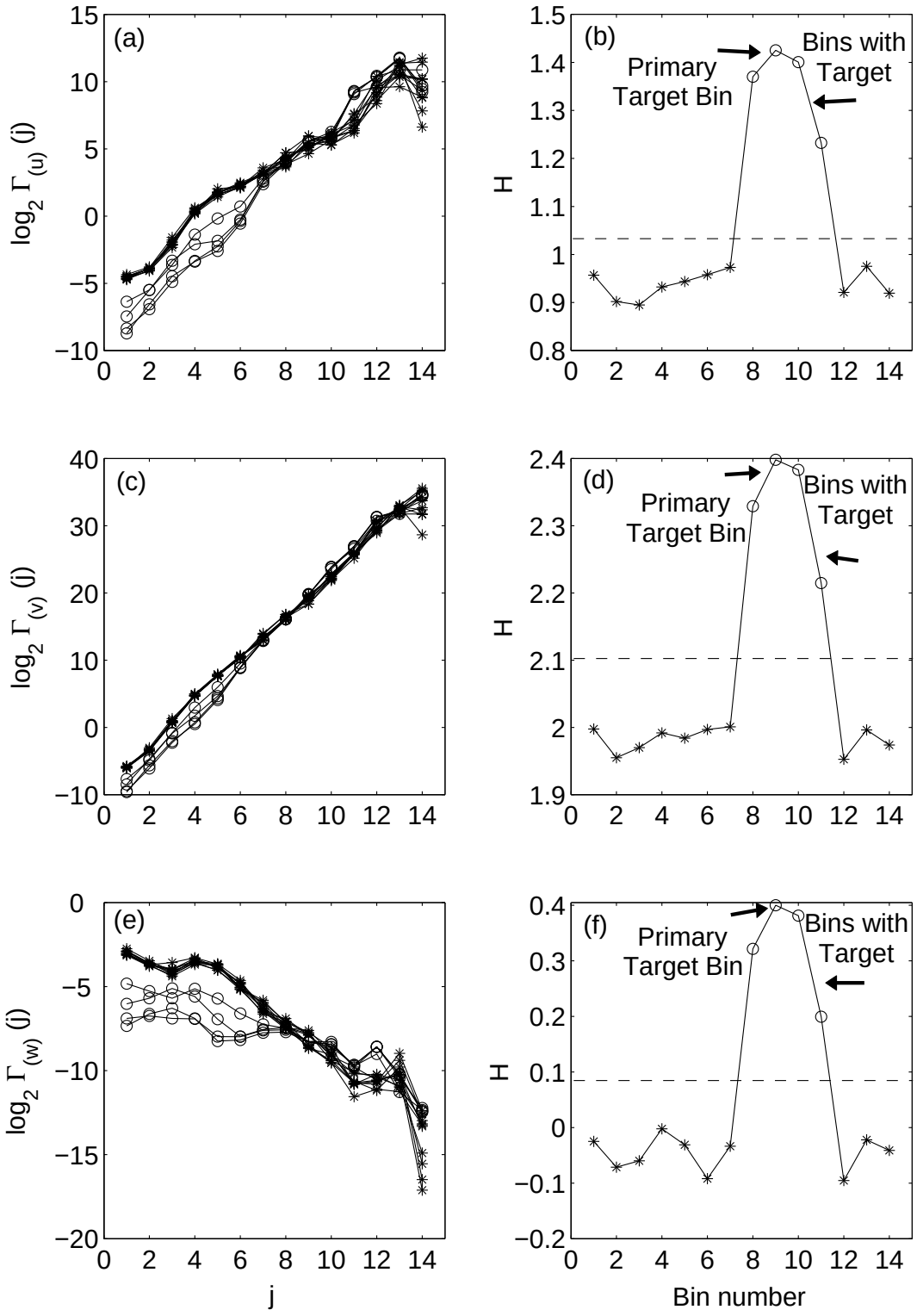

Figure 11:

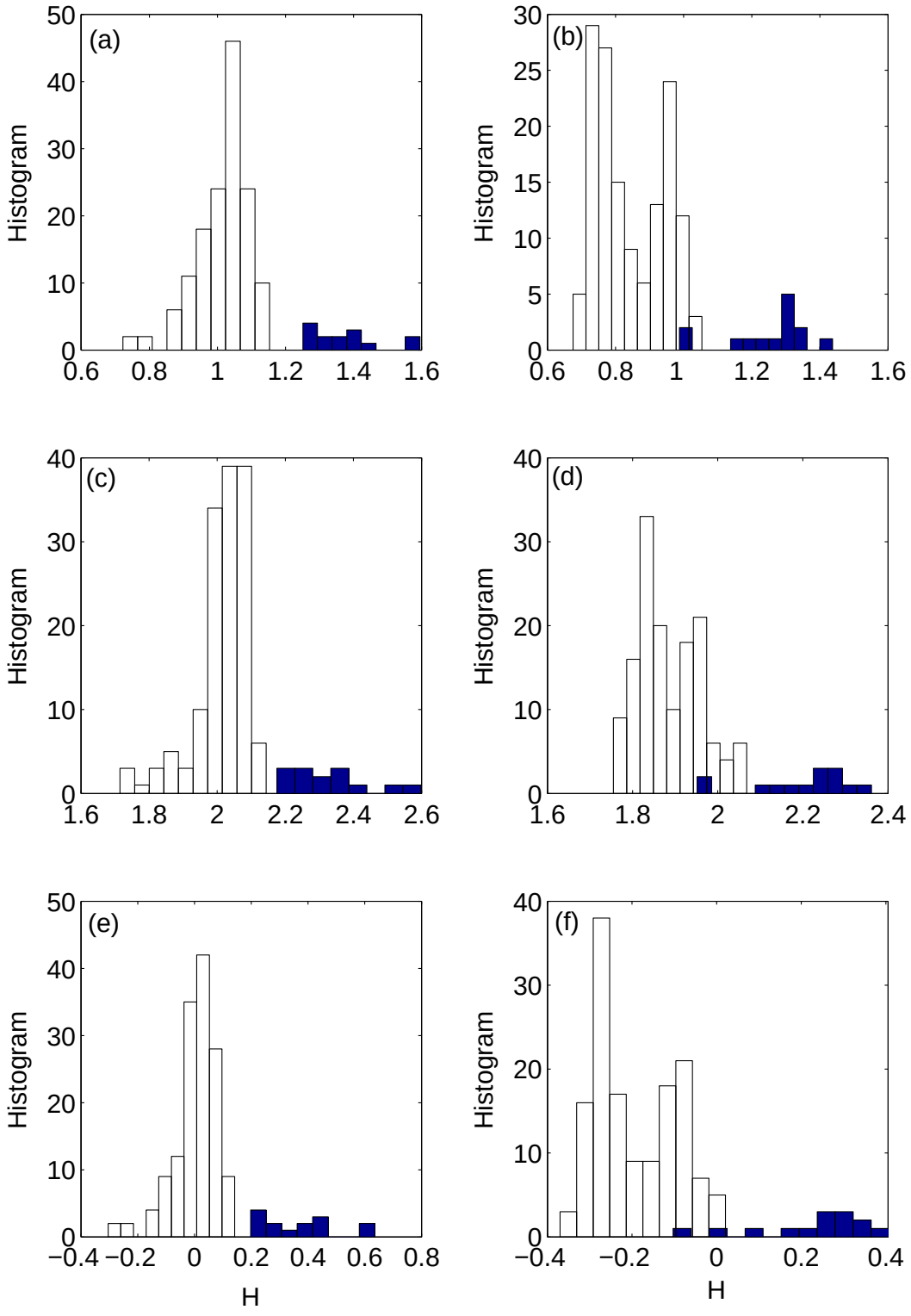

Figure 12:

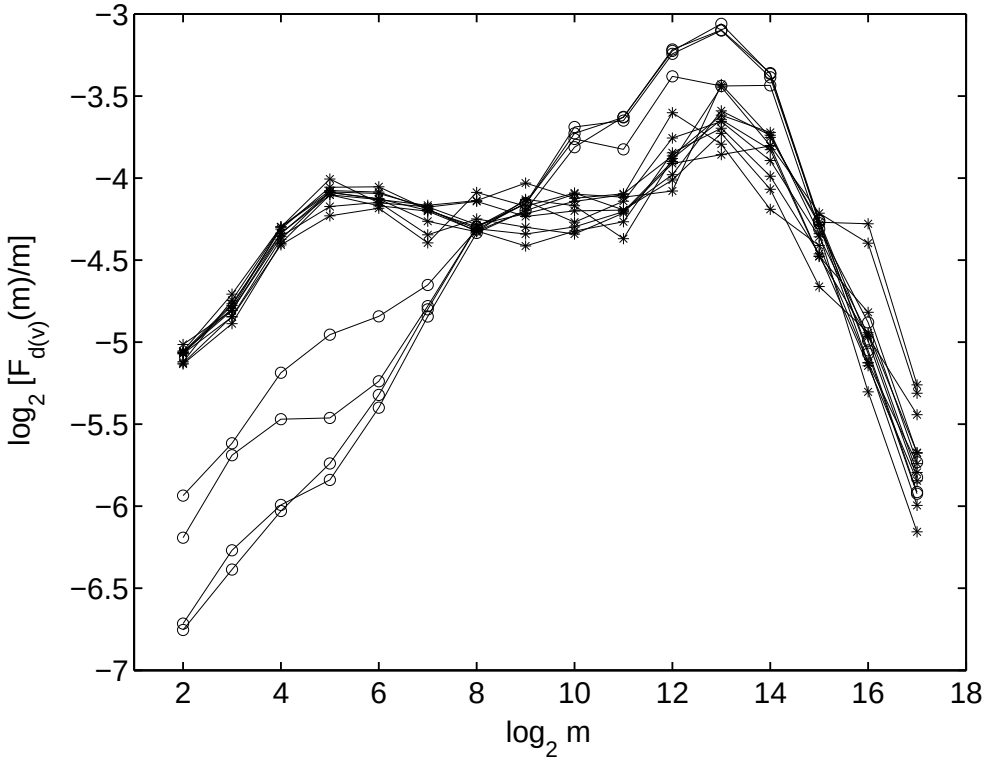

Figure 13: